Journal of Power Sources 196 (2011) 2785–2789

Contents lists available at ScienceDirect

Journal of Power Sources

journal homepage: www.elsevier.com/locate/jpowsour

Short communication

Hydrolytic dehydrogenation of ammonia borane catalyzed by carbon supported Co core–Pt shell nanoparticles

Xiaojing Yang, Fangyi Cheng, Zhanliang Tao, Jun Chen*

Institute of New Energy Material Chemistry and Key Laboratory of Advanced Energy Materials Chemistry (Ministry of Education), Nankai University, Tianjin, 300071, People's Republic of China

ARTICLE INFO

Article history:
Received 30 July 2010
Received in revised form
23 September 2010
Accepted 24 September 2010
Available online 1 October 2010

Keywords:
Co
Pt
Core–shell nanoparticles
Ammonia borane
Hydrolysis

ABSTRACT

Co core–Pt shell nanoparticles (denoted as $Co_{1-x}@Pt_x$ where $x = 0.33$, 0.43, 0.60, 0.68, 0.82) and carbon supported Co core–Pt shell nanoparticles (denoted as $Co_{1-x}@Pt_x/C$ where $x = 0.60$, 0.68, 0.82) ($Co_{1-x}@Pt_x/C = 43\%$), which are synthesized through a polyol reduction process with oleic acid as a surfactant, have been investigated as catalysts for hydrogen generation from hydrolysis of ammonia borane (NH_3BH_3) at $25 \pm 0.5\,^{\circ}C$. The as-prepared Co core–Pt shell nanoparticles are uniformly dispersed on carbon surface with diameters of about 3 nm. It is found that the catalysts show favorable performance toward the hydrolysis of NH_3BH_3 and the catalytic activity is associated with the ratio of Pt to Co. Among the catalysts studied, $Co_{0.32}@Pt_{0.68}/C$ ($Co_{0.32}@Pt_{0.68}/C = 43\%$) displays the highest catalytic performance, delivering a high hydrogen-release rate of 4874 mL min^{-1} g^{-1} (per catalyst).

1. Introduction

Ammonia borane ($NH_3{\cdot}BH_3$, AB) has recently been considered as a promising candidate for chemical hydrogen storage application due to its low molecular weight and high hydrogen content of 19.6 wt% [1]. There are several methods of dehydrogenation of AB, which can be broadly divided into two categories, namely thermolysis and hydrolysis. With appropriate catalysts, hydrolysis of AB can release as much as 3 mol H_2/1 mol AB at room temperature [2,3]. Thus, the catalysts are the dominant factor for the hydrolysis of AB [4]. It is found that Pt-based catalysts show the best catalytic performance in AB hydrolysis [3,5]. Yang and co-workers have prepared the carbon supported Pt–metal nanoparticles with diameters of about 5–20 nm by a chemical impregnation method. The hydrolytic activity of Pt alloy catalysts displays in the order of $PtRu > Pt_3Au > PtIr > PtCo > Pt_3Ni > PtCu > PtSn \sim Pt$ in terms of hydrogen generation rate and yield [6]. Considering both the catalytic performance and the catalyst cost, Pt–Co nanoparticles should be promising.

In recent years, much effort has been devoted to prepare core–shell structured composition because these materials have more excellent physical and chemical properties than that of their single-component materials [7]. The interaction between the two components in core–shell clusters introduces a mutual influence on neighboring atoms and leads to unique properties. Recently, Au@Co nanoparticles have been used as catalyst for in situ hydrolysis of AB [8]. However, few studies have been carried out on the core–shell Pt-based catalysts toward the hydrolysis of AB. Our interest is whether the catalytic activity of Pt–Co catalyst with Co core–Pt shell architecture can be increased by changing the architecture and the composition. It is therefore that in this work, different compositions of Co core–Pt shell nanoparticles ($Co_{1-x}@Pt_x$ NPs, $x = 0.33$, 0.43, 0.60, 0.68, and 0.82) and carbon supported Co core–Pt shell nanoparticles ($Co_{1-x}@Pt_x/C$ NPs, $x = 0.60$, 0.68, and 0.82) ($Co_{1-x}@Pt_x/C = 43\%$) with small sizes of several nanometers have been synthesized through a simple reduction process. Furthermore, the as-prepared core–shell NPs were investigated as the catalysts for the hydrolysis of AB.

2. Experimental

2.1. Catalyst preparation

The Co nanoparticles (Co NPs) were prepared by a polyol reduction process following modified procedures reported previously [9]. 20 mmol of cobalt acetate and 20 mmol of NaOH were mixed and stirred in deoxygenated ethylene glycol under Ar atmosphere. The solution was heated to 150 °C and then 20 mmol of oleic acid was added. The mixture was further heated to 200 °C and refluxed for 2 h. For comparison, micrometer-sized Co particles

* Corresponding author. Fax: +86 22 23506808.
E-mail address: chenabc@nankai.edu.cn (J. Chen).

0378-7753/$ – see front matter © 2010 Elsevier B.V. All rights reserved.
doi:10.1016/j.jpowsour.2010.09.079

(Co MPs) were also synthesized without adding oleic acid under the same process. The synthesized Co particles were centrifugated, washed with ethanol, and dried under vacuum at 60 °C for 12 h.

Co_{1-x}@Pt_x NPs (x = 0.33, 0.43, 0.60, 0.68, and 0.82) were chemically prepared through a reduction reaction method at room temperature. H_2PtCl_6 (50 mM in isopropanol) was slowly dripped to the Co NPs. The molar ratios of Co to H_2PtCl_6 were chosen at 14, 11, 9, 7, and 5 in order to obtain catalysts with different Pt contents. When the ratio of Co to H_2PtCl_6 was less than 2, pure Pt was prepared. The reduction reaction can be described as Eq. (1):

$$(1+x)Co + xPtCl_6^{2-} \rightarrow 2xCo^{2+} + Co_{1-x}@Pt_x + 6xCl^- \quad (1)$$

The $Co_{0.32}$@$Pt_{0.68}$ micrometer-sized particles ($Co_{0.32}$@$Pt_{0.68}$ MPs) with an average diameter of one micrometer were obtained through the same method as above by using Co MPs. The Co_{1-x}@Pt_x/C NPs (x = 0.60, 0.68, and 0.82) (Co_{1-x}@Pt_x/C = 43%) were prepared using similar method described above except that a certain amount of carbon black was added at 150 °C before the reduction reaction. When the ratio of Co to H_2PtCl_6 was 1/3, Pt/C (Pt/C = 43%) NPs were also prepared. The synthesized particles were precipitated by centrifugation and washed with ethanol for several times. Finally, the samples were dried under vacuum at 60 °C for 12 h.

2.2. Catalyst characterization

The as-synthesized catalysts were characterized by powder X-ray diffraction (XRD, Rigaku D/max-2500 X-ray generator, Cu Kα radiation), transmission electron microscopy equipped with energy dispersive X-ray spectroscopy microanalyzer (TEM and EDX, Philips Tecnai F20, 200 kV), and inductively coupled plasma emission spectroscopy (ICP).

2.3. Hydrogen generation measurement

The catalytic activities of the synthesized catalysts for hydrogen generation from the hydrolysis of AB solution were investigated at 25 ± 0.5 °C and atmosphere. The volume ($V_{(\text{generated H2, mL})}$) of the generated H_2 was measured by the water displacement method at 25 ± 0.5 °C [10]. AB solution and ~0.007 g catalysts were placed in a sealed flask fitted with an outlet tube for collecting the evolved H_2. The catalysis reaction was conducted without stirring because the Co or Co_{1-x}@Pt_x will stick to the magnetic stir. When the reaction goes on, the catalysts would be dispersed by the H_2 stream generated through the catalytic reaction. The exhaust equipment was placed under an inverted, water-filled gas burette and situated in a water-filled vessel [11]. The process of AB hydrolysis can simply be described as follows [3]:

$$NH_3BH_3 + 2H_2O \rightarrow NH_4^+ + BO_2^- + 3H_2 \quad (2)$$

The hydrogen generation rates (r) are calculated by $r = V_{(\text{generated H2, mL})}/(T_{(\text{time, min})} \times m_{(\text{the amount of the catalyst, g})})$ from the slops of the fitting lines that are obtained from the curves of the generated hydrogen volume vs time at different temperatures (25, 30, 35 and 40 °C) and below the hydrogen volume of 60 mL. Then, the rate constant (k) is determined by $k = (P_{(\text{the pressure, Pa})} \times r_{(\text{the rate, mL min}^{-1}\text{ g}^{-1})})/(8.314 \times T_{(\text{the temperature, K})})$. Finally, from the slop of the Arrhenius plot, the activation energy (E_a) can be decided.

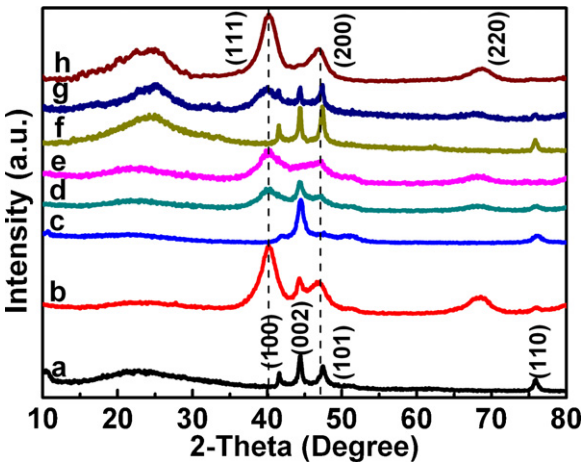

Fig. 1. XRD patterns of the catalysts: (a) Co MPs, (b) $Co_{0.32}$@$Pt_{0.68}$ MPs, (c) Co NPs, (d) $Co_{0.32}$@$Pt_{0.68}$ NPs, (e) Pt NPs, (f) Co/C NPs, (g) $Co_{0.32}$@$Pt_{0.68}$/C NPs, and (h) Pt/C NPs (metal/C = 43 wt%).

3. Results and discussion

3.1. Catalyst characterization

Fig. 1 shows the XRD patterns of the synthesized catalysts. Four characteristic diffraction peaks in curves a, c and f can be indexed as (1 0 0), (0 0 2), (1 0 1) and (1 1 0) crystal planes of hexagonal Co (JCPDS No. 89-7094). The particles with deposited Pt in curves b, d, e, g, and h display three new diffraction peaks corresponding to (1 1 1), (2 0 0), and (2 2 0) crystal planes of face-centered cubic Pt (JCPDS No. 87-647). The patterns of Co/C NPs, $Co_{0.32}$@$Pt_{0.68}$/C NPs, and Pt/C NPs (metal/C = 43%) samples present a broad peak at $2\theta = 25°$, which can be indexed to the vulcan carbon. In the present synthesis, the first step is the preparation of Co NPs by a surfactant-mediated polyol reduction process using oleic acid as a capping agent. The formation of the core–shell nanostructures is attained in the second step through the in situ reduction reaction method between Co NPs and $PtCl_6^{2-}$ (Eq. (1)). The driving force originates from the large standard redox potential difference between the Co^{2+}/Co (−0.280 V vs standard hydrogen electrode (SHE)) and the $PtCl_6^{2-}$/Pt (0.735 V vs SHE) redox pairs.

The microstructures of the obtained products were investigated by TEM analysis. It can be seen that the particles of $Co_{0.32}$@$Pt_{0.68}$ MPs are in spherical shape with diameter of about 1 μm (Fig. 2a). Co NPs and $Co_{0.32}$@$Pt_{0.68}$ NPs are uniformly distributed with sizes about 2–4 nm (Fig. 2c and e). For carbon supported samples, the metal particles are well-dispersed on the carbon surface and no obvious agglomeration can be observed (Fig. 2g). From HRTEM images of an individual particle (Fig. 2b, d, f, and h), the clear lattice fringes can be seen. Fig. 2f and h reveals that the core–shell structures consist of Co core for about 1 nm in diameter and the shell of Pt for about 2 nm. The Co NPs are well distributed with an average diameter of about 2.5 nm while $Co_{0.32}$@$Pt_{0.68}$ NPs possess the average size of 3.0 nm as seen from the size distribution histograms (Fig. 2i and j).

The compositions of the NPs were investigated by EDX and ICP analysis. The EDX spectra (Fig. 2k and l) of $Co_{0.32}$@$Pt_{0.68}$ NPs and $Co_{0.32}$@$Pt_{0.68}$/C NPs ($Co_{0.32}$@$Pt_{0.68}$/C = 43%) catalysts confirm the presence of Pt and Co, and the carbon signals in the EDX spectra are attributed to the carbon support. The ratio of metal to carbon is 43 wt% according to the EDX test. The determined elemental ratios tested by EDX are consistent with ICP results.

The EDX mapping of $Co_{0.32}$@$Pt_{0.68}$ MPs is shown in Fig. 2m–p so as to determine the Co@Pt core–shell architecture. Fig. 2m is the Ni map of the particles. The regions containing Ni are bright,

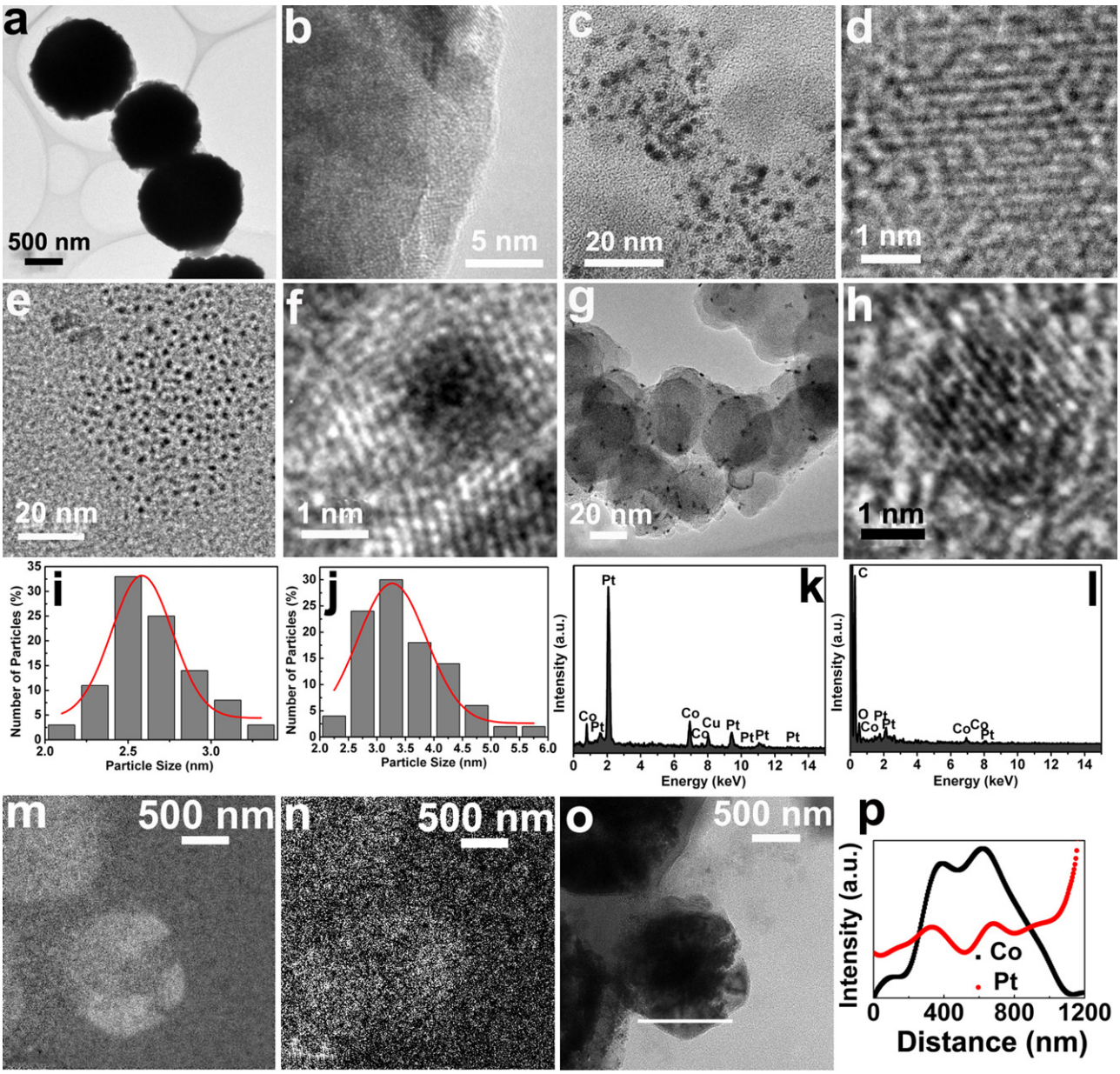

Fig. 2. TEM images of (a) $Co_{0.32}@Pt_{0.68}$ MPs, (c) Co NPs, (e) $Co_{0.32}@Pt_{0.68}$ NPs, (g) $Co_{0.32}@Pt_{0.68}$/C and the corresponding HRTEM images (b, d, f, h), size distributions for Co NPs (i) and $Co_{0.32}@Pt_{0.68}$ NPs (j), EDX spectrum for $Co_{0.32}@Pt_{0.68}$ NPs (k) and $Co_{0.32}@Pt_{0.68}$/C NPs (l), and EDX mapping images (m, n, o) and the line scanning analysis (p) for $Co_{0.32}@Pt_{0.68}$ MPs (metal/C = 43 wt%).

while other regions are dark in such an image. Fig. 2n is the Pt map, and the bright regions stand for the existence of Pt. The line scanning analysis data (Fig. 2o), marked by the white line in Fig. 2p, present the distributions of Pt and Co elements in the single particle. This analysis reveals that the intensity of Pt element is relatively high on the surface and low in the core of the particle while the Co element presents the reverse distribution. This character illustrates that the architecture of the sample is Co core–Pt shell. Thus, for $Co_{0.32}@Pt_{0.68}$ MPs, the shell (about 100 nm) is Pt and the core is Co. The same testing was made on $Co_{0.32}@Pt_{0.68}$ NPs, however, the NPs are too small to detect, and the loss energy of Pt is so vicious that the regions containing Pt are vague to be identified. The size histograms of Co NPs (Fig. 2i) and $Co_{0.32}@Pt_{0.68}$ NPs (Fig. 2j) show that the particle sizes increase by about 0.5 nm after Pt formation, which is in accordance with previous report that a Pt outer layer would enlarge the core–shell structure by less than 0.55 nm [12]. It is approved that on bulk Pt alloy surfaces, Pt can segregate in the outermost layer to form a "Pt-skin structure" which means that Pt is rich in the surface of Pt–Co alloy [13]. The formation of Co–Pt core shell NPs is also understood from the surface segregation prediction that Pt atoms are strongly enriched in the outermost of Pt (fcc)–M (hcp) alloy particles with sizes of 2.5–5.0 nm [14].

3.2. Catalytic activities

The hydrogen generation rates of the catalytic hydrolysis of AB are summarized in Table 1. The generated H_2 amount as a function of time with a certain amount of catalysts (catalyst/AB = 14 wt%) is shown in Fig. 3. The Co NPs exhibit almost no catalytic activity during the hydrolysis of AB, while the release of hydrogen is greatly quickened in the presence of Co@Pt catalysts. The synthesized $Co_{0.32}@Pt_{0.68}$ MPs show very low catalytic activities. However, the catalytic activities are greatly improved when the particle sizes are downsized into nanometer. The generation rates further increase

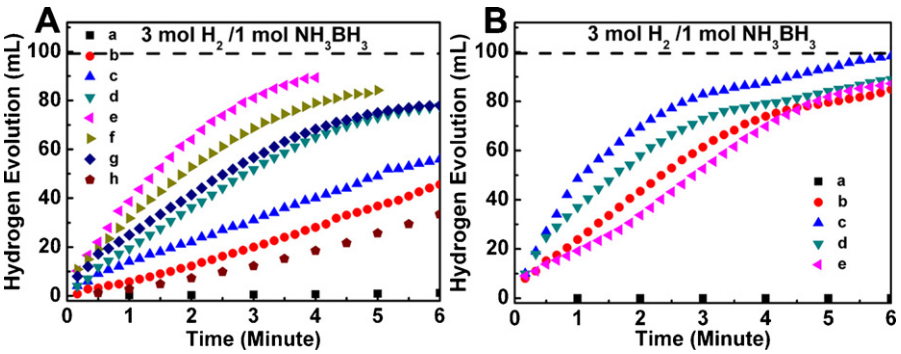

Fig. 3. Hydrogen generation from AB (0.5 wt%, 10 mL) containing different catalysts (catalyst/AB = 14 wt%) at 25 ± 0.5 °C and atmosphere: (A) Co_{1-x}@Pt_x NPs (a) x = 0, (b) x = 0.33, (c) x = 0.43, (d) x = 0.60, (e) x = 0.68, (f) x = 0.82, (g) x = 1, and (h) $Co_{0.32}$@$Pt_{0.68}$ MPs. (B) Co_{1-x}@Pt_x/C NPs (metal/C = 43 wt%) (a) C, (b) x = 0.60, (c) x = 0.68, (d) x = 0.82, (e) x = 1.

Table 1
The hydrogen generation rates and the molar ratios of the generated hydrogen to initial AB for different catalysts (metal/C = 43 wt%) at 25 ± 0.5 °C and room pressure.

Catalysts	The slop of the fitting line (mL min^{-1})	H_2 generation rate (mL min^{-1} g^{-1})
Co NPs	2.591	370.1
$Co_{0.67}$@$Pt_{0.33}$ NPs	7.630	1090
$Co_{0.57}$@$Pt_{0.43}$ NPs	9.499	1357
$Co_{0.40}$@$Pt_{0.60}$ NPs	16.67	2381
$Co_{0.32}$@$Pt_{0.68}$ NPs	32.63	4662
$Co_{0.18}$@$Pt_{0.82}$ NPs	24.49	3499
Pt NPs	18.18	2597
$Co_{0.30}$@$Pt_{0.70}$ MPs	6.364	909.1
C	0	0
$Co_{0.40}$@$Pt_{0.60}$/C NPs	19.71	2816
$Co_{0.32}$@$Pt_{0.68}$/C NPs	34.12	4874
$Co_{0.18}$@$Pt_{0.82}$/C NPs	25.56	3651
Pt/C NPs	19.47	2781

when the NPs are dispersed on carbon support. The hydrolytic rates of $Co_{0.32}$@$Pt_{0.68}$ NPs and $Co_{0.32}$@$Pt_{0.68}$/C NPs ($Co_{0.32}$@$Pt_{0.68}$/C = 43%) are 4662 and 4874 mL min^{-1} g^{-1}, respectively, even better than pure Pt and Pt/C (Pt/C = 43%). These values are much larger than that of Pt_3Co (~1380 mL min^{-1} g^{-1}) reported by Yang and co-workers [6].

The question needed to explain is why the core shell catalysts show favorable catalysis. It should be clarified by the mechanism of the hydrolysis reaction. As pointed out by Xu and Chandra, AB interacts with the surface of the catalyst to form an activated complex which dissociates upon attack of a water molecule to liberate H_2 [15]. A plausible mechanism of H_2 release in our case is presented in Fig. 4. As shown in the scheme, the release of H_2 is due to the attack of water on a transient M–H [16]. So the formation of the transient is the prerequisite for the hydrolytic reaction. It is considered that Pt shows the best catalysis performance in AB hydrolysis, and is the easiest to form the transient M–H [17]. The utilization of Pt atom is the determinate factor in the reaction. The core–shell catalysts should be one of the most effective architecture to use the surface of Pt atom sufficiently. Therefore, Co@Pt NPs show higher activity than that of Pt and other Pt-based bimetal catalysts.

It is noted that the activities of different catalysts vary with the elemental composition. The hydrogen release rates first raise and then fall with increasing Pt content, presenting a nearly normal distribution trend (Fig. 5). $Co_{0.32}$@$Pt_{0.68}$ NPs and $Co_{0.32}$@$Pt_{0.68}$/C NPs ($Co_{0.32}$@$Pt_{0.68}$/C = 43%), which are the peaks of the curves in Fig. 5, display the highest catalytic activity. The preliminary interpretations of the catalytic activity correlated with the compositions are as follows. For hydrolysis reaction, the release of H_2 is due to the attack of water on a transient M–H [15]. It has been reported that a volcano shape is found when the catalytic activity is plotted as a function of the strength of M–H bond [18,19]. Strong M–H bond does not mean favorable catalytic activity, but the suitable strength of M–H bond is good for catalysts. The strong adsorption affinity makes the production of the hydrolysis hard to leave and thus prevents the reaction. Pt belongs to the family of low hydrogen overpotential, which has strong adsorption affinity for hydrogen [6]. By introduction of Co into Pt, it is quite feasible to tune electronic surface properties [20], leading the bond with hydrogen weaker than that in pure Pt and then the increase of the catalytic activity. The same phenomenon has been detected in Pt–Ni alloy [6,21]. Our previous work has also demonstrated that the best performance is achieved when the content of Pt is about 65% in Pt–Ni alloy [21]. In this work, $Co_{0.32}$@$Pt_{0.68}$/C NPs ($Co_{0.32}$@$Pt_{0.68}$/C = 43%) shows the best activity.

In order to get the activation energy (E_a) of dehydrogenation reaction for $Co_{0.32}$@$Pt_{0.68}$/C NPs ($Co_{0.32}$@$Pt_{0.68}$/C = 43%), the

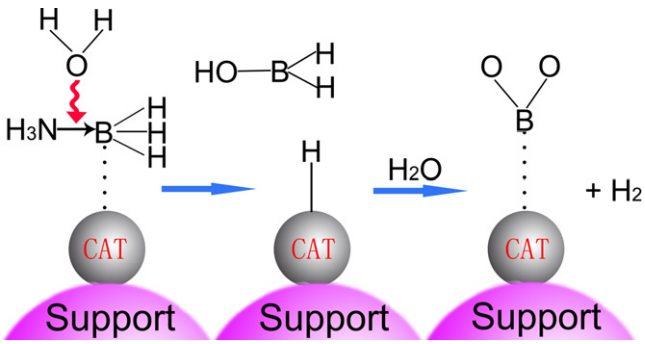

Fig. 4. The schematic diagram of metal catalyst for hydrogen generation from hydrolysis of AB.

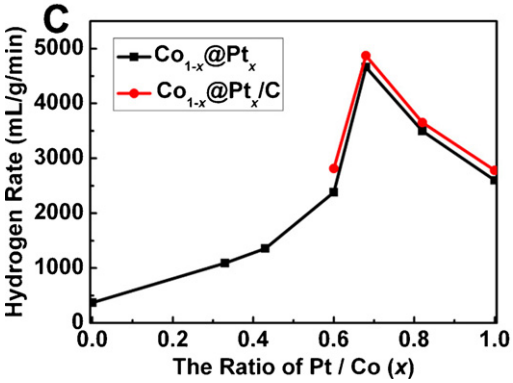

Fig. 5. The effect of the Pt content in Co_{1-x}@Pt_x and Co_{1-x}@Pt_x/C NPs (metal/C = 43 wt%) on the hydrolytic rates at 25 ± 0.5 °C and atmosphere.

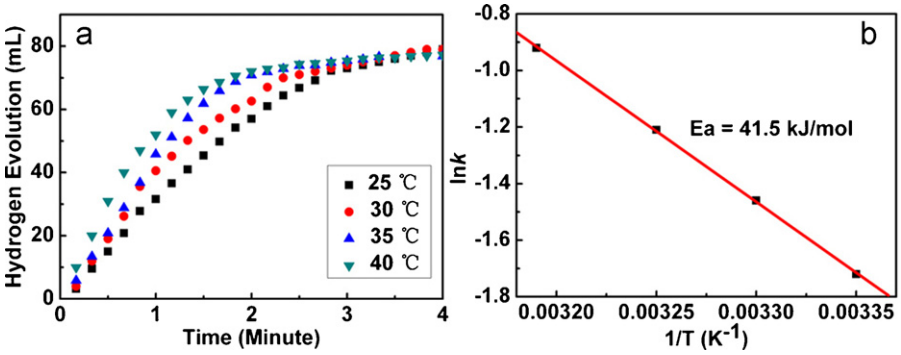

Fig. 6. (a) Temperature effect on hydrogen generation rate using a certain amount of $Co_{0.32}@Pt_{0.68}$/C NPs (catalyst/AB = 14 wt%) ($Co_{0.32}@Pt_{0.68}$/C = 43 wt%) in AB solution (0.5 wt%, 10 mL) at atmosphere and (b) the Arrhenius plots of ln k vs the reciprocal absolute temperature $1/T$.

Table 2
H_2 generation rates for the hydrolysis of AB catalyzed by $Co_{0.32}@Pt_{0.68}$/C NPs (metal/C = 43 wt%) (7 mg) at room pressure.

T (°C)	The slop of the fitting line (mL g^{-1})	r (mL g^{-1} min^{-1})	k (mol min^{-1} g^{-1})	$1/T$ (1/K)	ln k
25 ± 0.5	30.62	4375	0.179	0.00335	−1.72
30 ± 0.5	41.08	5869	0.232	0.00330	−1.46
35 ± 0.5	52.66	7523	0.298	0.00325	−1.21
40 ± 0.5	71.89	1.027×10^4	0.399	0.00319	−0.92

hydrolytic reactions at different temperatures were carried out. The hydrogen generation rates and rate constant k at various temperatures (T) are summarized in Table 2. Fig. 6a shows the effect of temperature on the hydrogen generation rates of the $Co_{0.32}@Pt_{0.68}$/C NPs ($Co_{0.32}@Pt_{0.68}$/C = 43%). The Arrhenius plot of ln k vs $1/T$ for the catalyst is plotted in Fig. 6b. The slope of the straight line in Fig. 6b gives apparent E_a of 41.5 kJ mol^{-1}. In comparison, E_a are 21 kJ mol^{-1} for Al_2O_3 supported Pt [22], 70 and 62 kJ mol^{-1} for Ni [23] and Co [15,24,25], respectively. While, E_a for $Pt_{0.65}Ni_{0.35}$ and $Ni_{0.88}Pt_{0.12}$ are 39 kJ mol^{-1} [21] and 30 kJ mol^{-1} [26], respectively. It has been proved that higher catalytic activity corresponds to smaller activation energy [27]. Therefore, E_a values of the bimetallic catalysts are higher than that of the active elements and lower than the ones of the less active elements.

4. Conclusion

Nanostructured $Co_{1-x}@Pt_x$ (x = 0.33, 0.43, 0.60, 0.68, 0.82) and $Co_{1-x}@Pt_x$/C (x = 0.60, 0.68, and 0.82) ($Co_{1-x}@Pt_x$/C = 43%) catalysts with an average particle diameter of about 3 nm have been synthesized by the surfactant-mediated polyol reduction process. The as-prepared nanoparticles were investigated as the catalysts for the hydrogen generation from AB hydrolysis. The results show that $Co_{0.32}@Pt_{0.68}$/C NPs ($Co_{0.32}@Pt_{0.68}$/C = 43%) present the highest catalytic activities with rapid hydrolytic rate and high hydrogen generation efficiency, even better than pure Pt/C. The reaction system consisting of AB and $Co_{1-x}@Pt_x$ or $Co_{1-x}@Pt_x$/C NPs may find applications in the field of on-board hydrogen supply.

Acknowledgments

This work was supported by the Research Programs of MOST (2009AA03Z224 and 2009AA05Z106), MOE (IRT-0927) and Tianjin High-Tech (08JCZDJC21300).

References

[1] S. Basu, Y. Zheng, A. Varma, W.N. Delgass, J.P. Gore, J. Power Sources 195 (7) (2010) 1957–1963.
[2] B. Peng, J. Chen, Energy Environ. Sci. 1 (4) (2008) 479–483.
[3] M. Chandra, Q. Xu, J. Power Sources 156 (2) (2006) 190–194.
[4] J.M. Yan, X.B. Zhang, H. Shioyama, Q. Xu, J. Power Sources 195 (4) (2010) 1091–1094.
[5] I.P. Jain, P. Jain, A. Jain, J. Alloys Compd., doi:10.1016/j.jallcom.2010.04.250.
[6] C.F. Yao, L. Zhuang, Y.L. Cao, X.P. Ai, H.X. Yang, Int. J. Hydrogen Energy 33 (10) (2008) 2462–2467.
[7] J. Sheng, S. Zhang, Y. Tong, Y. Liu, W.D. Sun, J. Alloys Compd. 473 (1–2) (2009) 477–482.
[8] J.M. Yan, X.B. Zhang, T. Akita, M. Haruta, Q. Xu, J. Am. Chem. Soc. 132 (15) (2010) 5326–5327.
[9] C.W. Kim, H.G. Cha, Y.H. Kim, A.P. Jadhav, E.S. Ji, D.I. Kang, Y.S. Kang, J. Phys. Chem. C 113 (13) (2009) 5081–5086.
[10] J.Z. Zhao, H. Ma, J. Chen, Int. J. Hydrogen Energy 32 (18) (2007) 4711–4716.
[11] X.W. Zhang, J.Z. Zhao, F.Y. Cheng, J. Liang, Z.L. Tao, J. Chen, Int. J. Hydrogen Energy 35 (15) (2010) 8363–8369.
[12] Y.M. Chen, F. Yang, Y. Dai, W.Q. Wang, S.L. Chen, J. Phys. Chem. C 112 (5) (2008) 1645–1649.
[13] S. Chen, P.J. Ferreira, W.C. Sheng, N. Yabuuchi, L.F. Allard, Y. Shao-Horn, J. Am. Chem. Soc. 130 (42) (2008) 13818–13819.
[14] G.F. Wang, M.A. Van Hove, P.N. Ross, M.I. Baskes, Prog. Surf. Sci. 7 (1) (2005) 28–45.
[15] Q. Xu, M. Chandra, J. Power Sources 163 (1) (2006) 364–370.
[16] G. Guella, C. Zanchetta, B. Patton, A. Miotello, J. Phys. Chem. B 110 (34) (2006) 17024–17033.
[17] J.E. Huheey, Inorganic Chemistry, 3rd ed., Harper & Row Publishers, New York, 1983, pp. 146–148.
[18] B.E. Conway, J.O.M. Bockris, J. Chem. Phys. 26 (1957) 532–541.
[19] R. Parsons, Trans. Faraday Soc. 54 (1958) 1053–1063.
[20] V.R. Stamenkovic, B.S. Mun, K.J.J. Mayrhofer, P.N. Ross, N.M. Markovic, J. Am. Chem. Soc. 128 (27) (2006) 8813–8819.
[21] X.J. Yang, F.Y. Cheng, J. Liang, Z.L. Tao, J. Chen, Int. J. Hydrogen Energy 34 (21) (2009) 8785–8792.
[22] M. Chandra, Q. Xu, J. Power Sources 168 (1) (2007) 135–142.
[23] S.B. Kalidindi, M. Indirani, B.R. Jagirdar, Inorg. Chem. 47 (16) (2008) 7424–7429.
[24] Ö. Metin, S. Özkar, Energy Fuels 23 (7) (2009) 3517–3526.
[25] K.S. Eom, M.J. Kim, R.H. Kim, D.H. Nam, H.S. Kwon, J. Power Sources 195 (9) (2010) 2830–2834.
[26] F.Y. Cheng, H. Ma, Y.M. Li, J. Chen, Inorg. Chem. 46 (3) (2007) 788–794.
[27] Q. Xu, M. Chandra, J. Alloys Compd. 446 (2007) 729–732 (special issue).